ISSN 0021-3640, JETP Letters, 2018, Vol. 107, No. 8, pp. 493–499. © Pleiades Publishing, Inc., 2018.
Published in Russian in Pis'ma v Zhurnal Eksperimental'noi i Teoreticheskoi Fiziki, 2018, Vol. 107, No. 8, pp. 512–518.

CONDENSED MATTER

Influence of Coulomb Correlations on Nonequilibrium Quantum Transport in a Quadruple Quantum-Dot Structure[1]

M. Yu. Kagan[a, b, *] and S. V. Aksenov[c, **]

[a] *Kapitza Institute for Physical Problems, Russian Academy of Sciences, Moscow, 119334 Russia*
[b] *National Research University Higher School of Economics, Moscow, 101000 Russia*
[c] *Kirensky Institute of Physics, Federal Research Center KSC, Siberian Branch, Russian Academy of Sciences, Krasnoyarsk, 660036 Russia*
**e-mail: kagan@kapitza.ras.ru*
***e-mail: asv86@iph.krasn.ru*

Received March 16, 2018

The description of quantum transport in a quadruple quantum-dot structure (QQD) is proposed taking into account the Coulomb correlations and nonzero bias voltages. To achieve this goal the combination of nonequilibrium Green's functions and equation-of-motion technique is used. It is shown that the anisotropy of kinetic processes in the QQD leads to negative differential conductance (NDC). The reason for the effect is an interplay of the Fano resonances, which are induced by the interdot Coulomb correlations. Different ways to increase the peak-to-valley ratio related to the observed NDC are discussed.

DOI: 10.1134/S0021364018080027

1. Technological development in recent decades allowed the experimental study of systems of few-electron quantum dots [1, 2]. In these structures the occupation of each dot and the interaction between them are governed by the electric fields of gate electrodes. Since the lifetime of single-electron spin state, a spin qubit, in semiconducting quantum dot is relatively long, such objects are attractive for storage and processing of quantum information [3, 4]. The research of quantum-dot complexes in this direction is necessary to create a scalable architecture of spin qubits [5, 6].

Intra- and interdot Coulomb interactions are the key factors determining different many-particle effects in the systems of quantum dots. They are being considered as a perfect testbed to study the properties of the Hubbard model due to the possibility of effective control of the internal parameters such as the interdot tunneling, single-electron energies and intensities of Coulomb interactions [7].

Nowadays, the structures consisting of three and four quantum dots are experimentally available and can be studied in different topologies. The dots can form a linear molecule where the nearest-neighbor tunneling of electrons takes place and the edge dots are disconnected from each other. Alternatively, such dots can be arranged in the shape of triangle or square, respectively. In this case, there is the nearest-neighbor coupling of all the dots [8–10]. The topology significantly affects the system properties. In particular, considering the Hubbard model with very large values of the intradot Coulomb repulsion U, it was shown that the presence of closed paths for the motion of electrons allows realization of Nagaoka ferromagnetic order [11, 12]. In case of quadruple quantum-dot structure (QQD) with three electrons, the appearance of ground state with spin $S = 3/2$ is explained by the presence of effective gauge field, which leads to an increase in the energy of chiral state with spin $S = 1/2$. This effect is one of the mechanisms that initiates a spin blockade of electron current through the QQD [13]. In this regime, the transitions between the states that differ in the number of electrons by 1 are forbidden if the spin of these states differs by more than 1/2. It should be noted that the spin blockade was also demonstrated earlier for double- and triple-linearly connected quantum dots [14, 15] and for a separate multi-level dot [16]. One of its manifestations in the observable values is a current rectification and a negative differential conductance (NDC). Among other mechanisms of current suppression in quantum-dot systems, one can mention the Aharonov–Bohm effect [17], the dark states [18–20], and the isospin blockade [21].

In this article, we propose an alternative description of the NDC effect observed in the transport properties of QQD. The investigated system is schematically shown in Fig. 1. The dots constituting the device are located at the vertices of square. The left and right

[1] The article is published in the original.

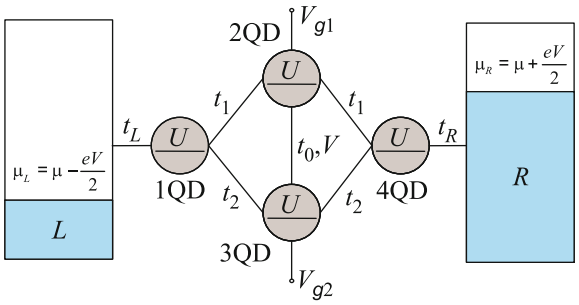

Fig. 1. (Color online) Quadruple quantum dot between the one-band paramagnetic leads.

metal contacts considered in the one-band approximation are connected to the first and fourth dots (1QD and 4QD), respectively. Thus, there are second and third dots (2QD and 3QD) in the central part of the QQD and two paths, top and bottom ones, for electron transport. The electron current is found by solving the systems of equations of motion for the nonequilibrium Green's functions. The NDC effect arising in the case of the anisotropic QQD is interpreted in terms of bound states in continuum (BICs) and the interaction of Fano resonances which are formed by the Coulomb correlations between the electrons of central dots, V.

2. The Hamiltonian of QQD between the metallic leads is $\hat{H} = \hat{H}_L + \hat{H}_R + \hat{H}_D + \hat{H}_T$. The terms $\hat{H}_L$ and $\hat{H}_R$ describe the left and right one-band leads, respectively, and have the form $\hat{H}_\alpha = \sum_{k\sigma}\xi_{k\sigma}c^+_{\alpha k\sigma}c_{\alpha k\sigma}$, where $c_{\alpha k\sigma}$ annihilates an electron with a wave vector k, spin projection σ, and energy $\xi_{k\sigma} = \epsilon_{k\sigma} - \mu$ ($\mu = 0$ is the chemical potential) in the αth lead ($\alpha = L, R$).

The QQD Hamiltonian reads

$$\hat{H}_{\text{QQD}} = \sum_{\sigma;j=1}^{4}\xi_{j\sigma}a^+_{j\sigma}a_{j\sigma} + U\sum_{j=1}^{4}n_{j\uparrow}n_{j\downarrow} + V\sum_{\sigma\sigma'}n_{2\sigma}n_{3\sigma'} + \sum_{\sigma}\Big[t_1\left(a^+_{1\sigma} + a^+_{4\sigma}\right)a_{2\sigma} + t_2\left(a^+_{1\sigma} + a^+_{4\sigma}\right)a_{3\sigma} + t_0a^+_{2\sigma}a_{3\sigma} + \text{H.c.}\Big], \quad (1)$$

where $a_{j\sigma}$ annihilates an electron with a spin projection σ and an energy $\xi_{j\sigma} = \epsilon_{j\sigma} - \mu$ on the level of jth dot; $t_{1,2}$ is the hopping parameter in the top (1QD–2QD–4QD) or bottom (1QD–3QD–4QD) arms (see Fig. 1); t_0 is the hopping parameter between the arms; and U and V are the intensities of intra- and interdot Coulomb repulsion, respectively.

The last term in the Hamiltonian $\hat{H}$ is responsible for the interaction between the subsystems,

$$\hat{H}_T = T_L(t)\sum_{k\sigma}c^+_{Lk\sigma}a_{1\sigma} + T_R(t)\sum_{k\sigma}c^+_{Rk\sigma}a_{4\sigma} + \text{H.c.}, \quad (2)$$

where $T_{L(R)}(t) = t_{L(R)}e^{\mp\frac{ieV}{2}t}$ is the coupling parameter of the QQD with the left (right) lead. Note that the time dependence in $T_{L(R)}(t)$ appears due to nonequilibrium conditions meaning that the electrochemical potentials, μ_L and μ_R, are different from each other, $\mu_R - \mu_L = eV$ [22]. In subsequent calculations of the current and conductance, we consider symmetric transport regime, $t_L = t_R = t$.

3. The operator of steady-state electric current is defined as $\langle I(t,t)\rangle \equiv I = e\langle\dot{N}_L\rangle$, where $N_L = \sum_{k\sigma}c^+_{Lk\sigma}c_{Lk\sigma}$ is the left-lead particle operator. Writing the equation of motion one can get ($\hbar = 1$)

$$I = ie\sum_{k\sigma}\left[T^+_L(t)G^{+-}_{Lk1\sigma}(t,t) - T_L(t)G^{+-}_{1Lk\sigma}(t,t)\right]. \quad (3)$$

The nonequilibrium Green's functions are introduced in Eq. (3). The operators $c_{\alpha k\sigma}, a_{j\sigma}$ entering into them are ordered on the Keldysh contour, C [23].

If (2) is treated as an interaction operator than the analysis of perturbation-theory series for the functions $G^{+-}_{Lk1\sigma}$ and $G^{+-}_{1Lk\sigma}$ results in the following formula for the current,

$$I = e\sum_{\sigma}\int_C d\tau_1[\Sigma^{+a}_{L\sigma}(t-\tau_1)G^{a-}_{11\sigma}(\tau_1 - t) - G^{+a}_{11\sigma}(t-\tau_1)\Sigma^{a-}_{L\sigma}(\tau_1 - t)], \quad (4)$$

where the self-energy functions are introduced, $\Sigma^{ab}_{L\sigma}(\tau-\tau') = T^+_L(\tau)\sum_k g^{ab}_{Lk\sigma}(\tau-\tau')T_L(\tau')$, which characterize the influence of the left lead on the QQD; and $g^{ab}_{Lk\sigma}(\tau-\tau')$ is the one-electron Green's function of the left lead. The value of upper indices, $a, b = +, -$, points out the branch of Keldysh contour, C_+, C_-. The general form of the Dyson equation for the Green's function $G_{11\sigma}(\tau-\tau')$ is

$$G_{11\sigma}(\tau-\tau') = g_{11\sigma}(\tau-\tau') + \iint_C d\tau_1\tau_2[g_{11\sigma}(\tau-\tau_1)\Sigma_{L\sigma}(\tau_1-\tau_2)G_{11\sigma}(\tau_2-\tau') + g_{14\sigma}(\tau-\tau_1)\Sigma_{R\sigma}(\tau_1-\tau_2)G_{41\sigma}(\tau_2-\tau')], \quad (5)$$

where $g_{ij\sigma}(\tau-\tau')$ is the bare Green's functions of the QQD. During the derivation of Eqs. (4) and (5), we deal with the nonmagnetic approximation. Specifically, the spin-flip processes are neglected, $\langle a_{i\sigma}a^+_{j\bar{\sigma}}\rangle = 0$. After the transition to integration over the

real time contour and the subsequent Fourier transform, we obtain the expression

$$I = i\Gamma\sum_{\sigma}\int_{-\infty}^{+\infty} d\omega\Big[f_L\left(G^a_{11\sigma} - G^r_{11\sigma}\right) - G^{+-}_{11\sigma}\Big], \qquad (6)$$

where $f_L \equiv f\left(\omega + \dfrac{eV}{2}\right)$ is the Fermi–Dirac distribution function and $\Gamma/2 = \Gamma_L = \Gamma_R = \pi t^2 g$ is the parameter that describes the broadening of QQD levels due to the coupling with the leads. In general, the density of states of lead depends on frequency and spin projection, $g_\sigma(\omega) = \sum_k \delta(\omega - \xi_{k\sigma})$. However, in the article the leads are supposed to be paramagnetic and have wide band. Consequently, these dependences can be ignored and $g = \text{const}$. As a result, the Fourier transforms of self-energy functions of αth lead are $\Sigma^r_{\alpha\sigma} = -\dfrac{i}{2}\Gamma$ and $\Sigma^{+-}_{\alpha\sigma} = i\Gamma f_\alpha$.

To obtain the final expression describing the steady-state current in the system let us find the Green's functions of the QQD entering into (6). For this purpose, we use the equation-of-motion technique. The general form of equations for $G^r_{i\sigma j\sigma'}(\omega) \equiv \langle\langle a_{i\sigma}|a^+_{j\sigma'}\rangle\rangle^r$ and $G^{+-}_{i\sigma j\sigma'}(\omega) \equiv \langle\langle a_{i\sigma}|a^+_{j\sigma'}\rangle\rangle^{+-}$ differs from each other because of the definition of $G^{r,+-}_{i\sigma,j\sigma'}(t-t')$,

$$z\left\langle\left\langle a_{i\sigma}|a^+_{j\sigma'}\right\rangle\right\rangle^r = \left\{\left\langle a_{i\sigma}, a^+_{j\sigma'}\right\rangle\right\} + \left\langle\left\langle\left[a_{i\sigma}, \hat{H}\right]|a^+_{j\sigma'}\right\rangle\right\rangle^r,$$
$$z\left\langle\left\langle a_{i\sigma}|a^+_{j\sigma'}\right\rangle\right\rangle^{+-} = \left\langle\left\langle\left[a_{i\sigma}, \hat{H}\right]\mid a^+_{j\sigma'}\right\rangle\right\rangle^{+-},$$

where $z = \omega + i\delta$. In addition, taking into account the diagram expansion of mixed Green's function, $G_{L(R)kj\sigma}(t-t') = \int_C g_{L(R)kj\sigma}(t-\tau)T_{L(R)}(\tau)G_{1(4)j\sigma}(\tau - t')$, the corresponding equations become

$$z\left\langle\left\langle c_{L(R)k\sigma}|a^+_{j\sigma}\right\rangle\right\rangle^r = g^r_{L(R)k\sigma}t_{L(R)}\left\langle\left\langle a_{1(4)\sigma}|a^+_{j\sigma}\right\rangle\right\rangle^r,$$
$$z\left\langle\left\langle c_{L(R)k\sigma}|a^+_{j\sigma'}\right\rangle\right\rangle^{+-} = t_{L(R)}\Big(g^r_{L(R)k\sigma}\left\langle\left\langle a_{1(4)\sigma}|a^+_{j\sigma}\right\rangle\right\rangle^{+-} + g^{+-}_{L(R)k\sigma}\left\langle\left\langle a_{1(4)\sigma}|a^+_{j\sigma}\right\rangle\right\rangle^{a}\Big),$$

where $g^r_{\alpha k\sigma} = (z - \xi_{k\sigma})^{-1}$, $g^{+-}_{\alpha k\sigma} = 2\pi i f_\alpha \delta(\omega - \xi_{k\sigma})$. Next, to derive the closed systems of equations we use the decoupling procedure for the nonmagnetic case developed in the [24–26]. Such an approximation is valid at temperatures higher than the Kondo temperature [27]. In the employed approach the equations for the third-order Green's functions, e.g., $\left\langle\left\langle n_{3\sigma}n_{2\bar\sigma}a_{2\sigma}|a^+_{j\sigma}\right\rangle\right\rangle^{r,+-}$, should be decoupled. The solution of the final set of equations for the retarded Green's functions is

$$G^r_{\beta\beta} = \frac{C_\beta Z_{\bar\beta}}{Z}, \quad G^r_{\beta\bar\beta} = \frac{C_\beta C_{\bar\beta}x_2}{Z}, \quad G^r_{\alpha\alpha} = \frac{C_\alpha\Delta_{\bar\alpha}}{Z}, \qquad (7)$$
$$G^r_{\alpha\bar\alpha} = \frac{C_\alpha C_{\bar\alpha}\Delta_1}{Z}, \quad G^r_{\beta\alpha} = \frac{C_\alpha C_\beta T_{\bar\beta}P_{\bar\alpha}}{Z},$$
$$\beta(\alpha) = 1, 4(2, 3),$$

where $\Delta_\alpha = D_\alpha T_\beta T_{\bar\beta} - t^2(\alpha)C_\alpha S$, $\Delta_1 = t_0 T_\beta T_{\bar\beta} + t(\alpha)t(\bar\alpha)S$, $S = C_\beta T_{\bar\beta} + C_{\bar\beta}T_\beta$, $P_\alpha = t(\bar\alpha)D_\alpha + t_0 t(\alpha)C_\alpha$, $Z = T_\beta T_{\bar\beta}x_1 - Sx_2$, $Z_\beta = T_\beta x_1 - C_\beta x_2$, $T_\beta = D_\beta + i\Gamma C_\beta/2$, $x_1 = \Delta_\alpha\Delta_{\bar\alpha} - t_0^2 C_\alpha C_{\bar\alpha}$, $x_2 = t(\alpha)C_\alpha P_{\bar\alpha} + t(\bar\alpha)C_{\bar\alpha}P_\alpha$, $t(\alpha) = t_{1,2}$. The factors $C_{\alpha,\beta}$ and $D_{\alpha,\beta}$ contain the explicit dependences on the occupation numbers, correlators and intensities of the Coulomb interactions in the QQD: $C_\alpha = C_{\alpha 1} + C_{\alpha 2}$, $C_{\alpha 1} = b_{\alpha 4}(b_{\alpha 2}b_{\alpha 3} + Ub_{\alpha 3}\langle n_\alpha\rangle + 2Vb_{\alpha 2}\langle n_{\bar\alpha}\rangle$, $C_{\alpha 2} = UV(b_{\alpha 2} + b_{\alpha 3})\left(2\langle n_\alpha\rangle\langle n_{\bar\alpha}\rangle - \langle a^+_\alpha a^-_{\bar\alpha}\rangle^2\right)$, $C_\beta = b_{\beta 2} + U\langle n_{\bar\beta}\rangle$, $D_\alpha = b_{\alpha 1}b_{\alpha 2}b_{\alpha 3}b_{\alpha 4}$, $D_\beta = b_{\beta 1}b_{\beta 2}$, $b_{\alpha 1} = z - \xi_\alpha$, $b_{\alpha 2} = b_{\alpha 1} - U$, $b_{\alpha 3} = b_{\alpha 1} - V(1 + \langle n_{\bar\alpha}\rangle)$, $b_{\alpha 4} = b_{\alpha 3} - U$. Note that the spin indices in Eqs. (7) are omitted for simplicity as in the nonmagnetic case we have $\langle a^+_{i\sigma}a_{j\sigma}\rangle = \langle a^+_{i\bar\sigma}a_{j\bar\sigma}\rangle$. In turn, the solution of the system of equations for G^{+-}_{ij} gives

$$G^{+-}_{\beta\beta(\bar\beta)} = i\Gamma\frac{C_\beta\left(f_\beta Z_{\bar\beta}G^a_{\beta\beta(\bar\beta)} + f_{\bar\beta}C_{\bar\beta}x_2G^a_{\bar\beta\beta(\bar\beta)}\right)}{Z},$$
$$G^{+-}_{\alpha\alpha(\bar\alpha)} = i\Gamma\frac{C_\alpha P_{\bar\alpha}\left(f_\beta C_\beta T_{\bar\beta}G^a_{\beta\alpha(\bar\alpha)} + f_{\bar\beta}C_{\bar\beta}T_\beta G^a_{\bar\beta\alpha(\bar\alpha)}\right)}{Z}, \qquad (8)$$
$$G^{+-}_{\beta\alpha} = i\Gamma\frac{C_\beta\left(f_\beta Z_{\bar\beta}G^a_{\beta\alpha(\bar\beta)} + f_{\bar\beta}C_{\bar\beta}x_2G^a_{\bar\beta\alpha(\bar\beta)}\right)}{Z},$$

where $f_\beta = f_{L,R}$, $G^a_{ij} = (G^r_{ij})^*$, $G^{+-}_{ij} = -(G^{+-}_{ji})^*$. Proceeding from the definition of lesser Green's functions the correlators and occupation numbers can be obtained by self-consistent solution of the following integral equations

$$\langle n_i\rangle = 2\int_{-\infty}^{+\infty}\frac{d\omega}{2\pi}G^{+-}_{ii}, \quad \left\langle a^+_i a_j\right\rangle = 2\int_{-\infty}^{+\infty}\frac{d\omega}{2\pi}G^{+-}_{ji}. \qquad (9)$$

Substituting the calculated Green's functions into Eq. (6), we find the final expression describing the current in the QQD,

$$I = 2e\Gamma^2\int_{-\infty}^{+\infty}d\omega G^r_{14}G^a_{41}(f_L - f_R)$$
$$= 2e\Gamma^2\int_{-\infty}^{+\infty}d\omega\frac{C_1^2C_4^2x_2^2}{|Z|^2}(f_L - f_R). \qquad (10)$$

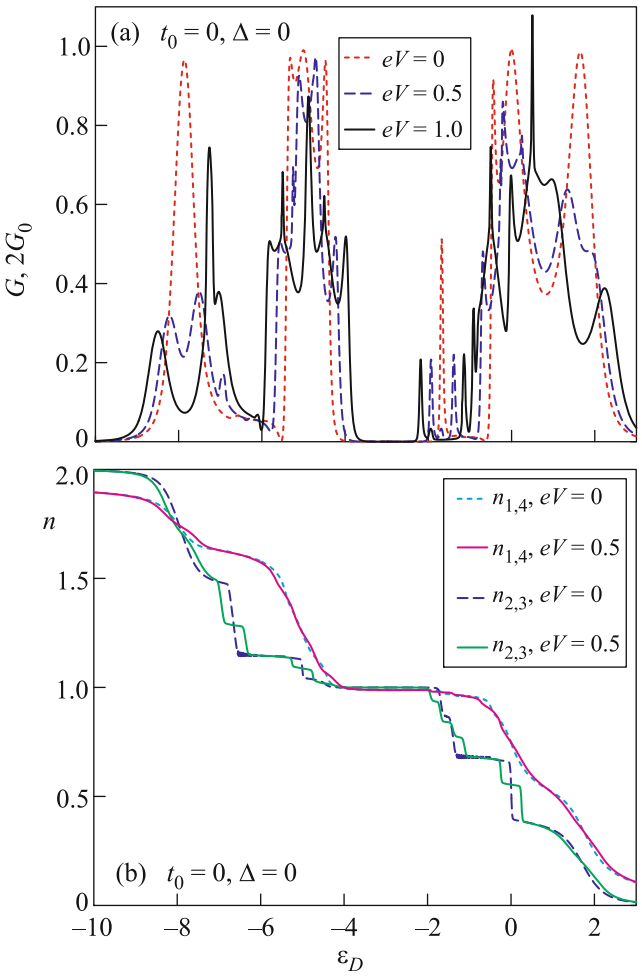

Fig. 2. (Color online) Effect of bias voltage on the gate-voltage dependences of (a) conductance and (b) occupation numbers for the isotropic quadruple quantum dot. Parameters: $U = 5$, $V = 1$, $t_1 = t_2 = 1$, $t_0 = \Delta = 0$, $k_B T = 0.01$.

Note that a factor of 2 in the numerators of Eqs. (9) and (10) arises because of the summation over the spin indices. In further discussion, all the energy values are measured in units of Γ. Additionally, the regime of strong coupling with contacts will be analyzed ($\Gamma = t_1$). In subsequent calculations, one-electron energies of the edge dots are assumed to be the same, $\xi_{1\sigma} = \xi_{4\sigma} = \varepsilon_D$. The difference of energies of two central dots is controlled by the parameter Δ, $\xi_{2(3)\sigma} = \varepsilon_D \pm \Delta$.

4. We now turn to the description of nonequilibrium transport through the QQD. Figures 2a and 2b show the conductance of QQD and its occupation numbers as functions of gate field at different bias voltages for the isotropic case, $t_1 = t_2$. It is seen that the resonances of $G(\varepsilon_D)$, which are located left and right from the insulating band (that corresponds to the half-filling), are split in comparison with the equilibrium regime (compare, e.g., dotted and dashed curves in Fig. 2a). It can be explained by the fact that for $eV \neq 0$ the transmission of electrons is enhanced if the QQD energy level governed by the parameter ε_D coincides with the electrochemical potential of the left or right lead, $\mu_{L,R} = \mu \mp \frac{eV}{2}$. Simultaneously, the Fano antiresonances in the conductance emerging due to the Coulomb interaction between the central dots [25, 26] are modified if $eV \neq 0$. Both insulating bands obtained in the linear response regime persist at $eV = 0.5$. However, the further increase in bias voltage gives rise to the decrease in the band widths (solid curve in Fig. 2a). Moreover, in strongly nonequilibrium regime, effects that cannot be described by the Landauer–Buttiker formula may appear. As a result, $G > 2G_0$ for some gate voltages in the situation when $\Gamma \sim U, V$. The steps of occupation numbers are also split at $eV \neq 0$ which is especially evident for the populations of two internal dots (Fig. 2b). In this case, each step corresponds to the conductance resonance.

Let us pass to the anisotropic situation, $t_1 \gg t_2$. The Fig. 3a represents the modification of gate-voltage dependence of conductance in this regime when the bias voltage is turned on. It is seen that the anisotropy of the kinetic processes in the QQD causes the appearance of conductance antiresonances with negative values. In Fig. 3b, the dotted curve shows the I–V characteristic in the gate field $\varepsilon_D = -0.82$ corresponding to the antiresonance of the highest amplitude in Fig. 3a. The I–V curve has four sections where the behavior of conductance differs substantially. At source–drain field energies $|eV| \leq 0.75$, the current practically does not increase analogously to the Coulomb blockade effect. At $0.75 \leq |eV| \leq 1$ the significant growth takes place followed by a sharp decline at $|eV| \approx 1$ with a narrow valley. At $1 \leq |eV| \leq 1.5$ the current considerably increases as well as in the second section. The peak-to-valley ratio in this case is ~1.4. The similar scenario is observed if the QQD occupation is above half-filling (dashed curve in Fig. 3b). The peak-to-valley ratio can be additionally increased if we take into account the hopping between the central dots and make their single-electron energies different by means of several gate electrodes ($t_0 \neq 0, \Delta \neq 0$). The I–V characteristic corresponding to this case is represented by a solid curve in Fig. 3b. It is clearly seen that the valley is wider and the peak-to-valley ratio is ~1.9. In the situation of T-shaped QQD geometry ($t_2 = 0$) the peak-to-valley ratio is ~2.6. For the $\Gamma \ll U, V$ mode and using the same relations between the hopping parameters t_1, t_2, t_0 as in Fig. 3, we can get the ratio of about 4 (the last two cases are not represented in Fig. 3).

The observed NDC effect is related to the features of density of states (DOS) of the QQD in the anisotro-

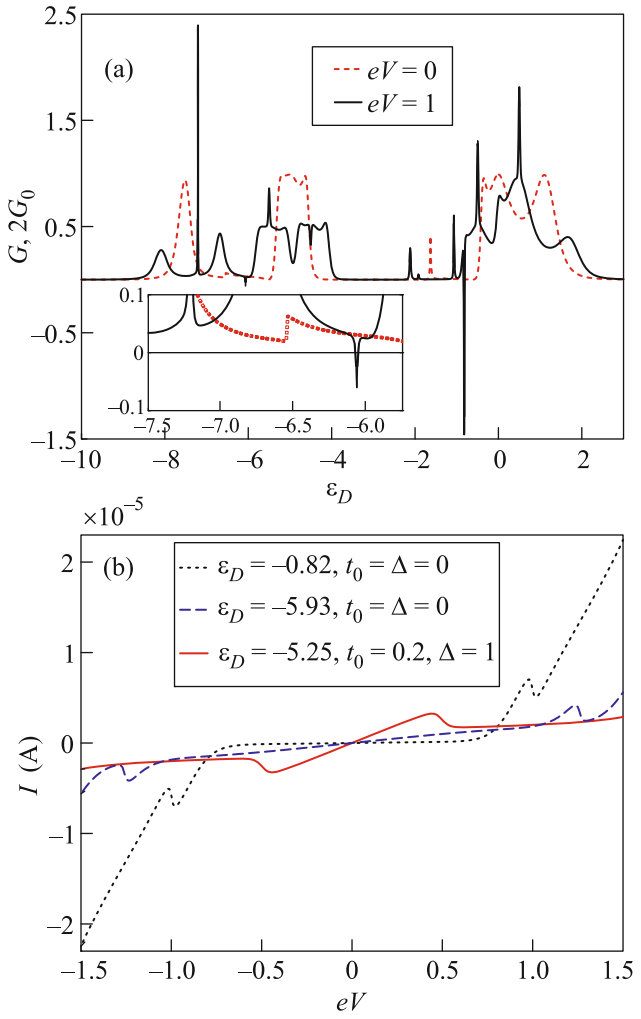

Fig. 3. (Color online) Transport properties of the anisotropic quadruple quantum dot. (a) Gate-voltage dependence of the conductance. Inset: the Fano antiresonance and its splitting at $eV \neq 0$. (b) Current–voltage characteristics. Parameters: $t_1 = 1$, $t_2 = 0.1$, the other parameters coincide with the ones used in Fig. 2.

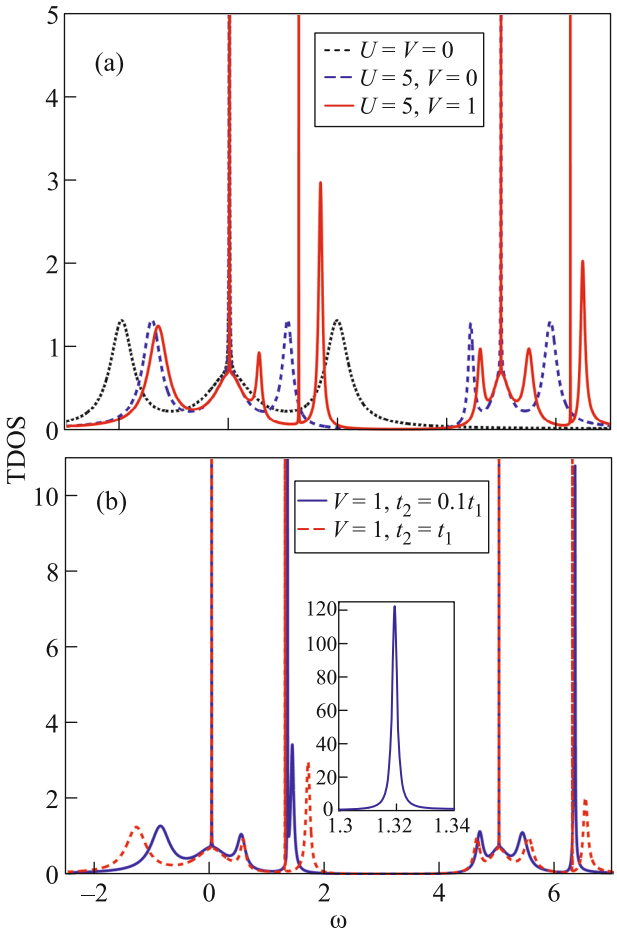

Fig. 4. (Color online) (a) Influence of Coulomb correlations on the bound states in continuum in the density of states of the isotropic quadruple quantum dot. (b) Effect of anisotropy of kinetic processes in the quadruple quantum dot on the bound states in continuum. Inset: one of the maxima related to the bound state in continuum, which is formed at $V \neq 0$. Parameters: $\varepsilon_D = 0$, the other parameters coincide with the ones used in Fig. 3.

pic regime, $\mathrm{TDOS}(\omega) = -\frac{1}{\pi}\sum_{i=1}^{4} \mathrm{Im}\{G_{ii}^r(\omega)\}$. First, we start with the isotropic situation. The appropriate DOS is displayed in Fig. 4a. In the absence of Coulomb interactions, the positions of maxima of $\mathrm{TDOS}(\omega)$ are determined by the energies of eigenstates of Hamiltonian $H_{QQD}(U = V = 0)$ (dotted curve in Fig. 4a). If $t_0 = \Delta = 0$ that there are four levels with the energies: ε_D, $\varepsilon_D \pm 2t_1$. As it was shown in [28, 29], the presence of the degeneracy can give rise to BICs. In our case, the BIC is displayed by the infinitely narrow peak at $\omega = 0$ whose width is characterized by the term $i\delta$ in $G_{ij}^r(\omega)$. Switching on the intradot Coulomb interactions results in the appearance of three new maxima due to the splitting of single-electron excitation energies of the individual dot: ε_D, $\varepsilon_D + U$ (dashed curve in Fig. 4a). As a consequence, the additional BIC occurs [30]. The interdot Coulomb interaction causes the extra splitting of one-electron excitation energies. Thus, two new maxima and two BICs arise in the DOS (solid curve in Fig. 4a). It is worth to note that these maxima are the reason for the conductance resonances in the linear response regime (dotted curve in Fig. 2a). In particular, the induction of asymmetric Fano peaks at $V \neq 0$ is attributed to the appearance of corresponding maxima in the dependence $\mathrm{TDOS}(\omega)$ [25, 26]. In turn, the BICs do not manifest themselves in the QQD transport characteristics.

In the anisotropic situation, the lifetime of two BICs induced by the interdot Coulomb correlations becomes finite. As a result, two narrow peaks of finite height emerge (solid curve in Fig. 4b and the inset)

and new Fano antiresonances appears in the conductance. One of them is shown in the inset of Fig. 3a at $\varepsilon_D \approx -6.5$ (see dotted curve). The nonzero value of G is due to the temperature factor. It was already mentioned above that the conductance resonances are split in the nonequilibrium regime. In turn, the antiresonance under consideration is transformed into a narrow resonance and antiresonance with $G > 0$ and $G < 0$, respectively. They are placed at the distance of approximately eV (in the inset of Fig. 3a the bottom of resonance and the antiresonance at $eV \neq 0$ are plotted by solid curve). The increase in bias voltage shifts the antiresonance to the right. Simultaneously, the Fano asymmetric peak arising at $V \neq 0$ in the isotropic case is shifted to the left. Thus, the amplification of NDC is observed when preformed Fano features are close to each other and interact. The described scenario is also realized if the QQD occupation is less than one half.

Note that in [31], where a parallel-coupled double quantum dot is studied, the NDC effect induced by the Coulomb correlations occurs if the dots are connected with the leads asymmetrically. In our case, the NDC takes place in the symmetric coupling regime. At the same time, the asymmetry of kinetic processes, leading to the above-mentioned peculiarities in the DOS and specific redistribution of dots' occupations, is a property of the device itself.

5. In this article, we investigated the influence of nonequilibrium effects on quantum transport in a system of four quantum dots taking into account the Coulomb correlations. To find the expression that describes the electron current the nonequilibrium Green's functions and equation-of-motion technique are applied. In the last case, the equations for the third-order Green's functions were decoupled [32] as it had been described earlier in [24–26]. The numerical analysis of the QQD DOS showed that the system contains the BICs induced by the Coulomb interactions. It is shown that the anisotropy of kinetic processes in the QQD results in the finite lifetime of BICs, which are created by the interdot Coulomb interaction. The consequent Fano antiresonances in the gate-voltage dependence of the conductance are shifted in nonequilibrium regime. The interaction of these features with the other Fano asymmetric peaks (which are caused by the interdot Coulomb correlations and appear even in the isotropic case) gives rise to significant enhancement of the NDC effect. It is demonstrated that the corresponding peak-to-valley ratio of the I–V characteristic can be significantly increased by the change of the system parameters.

We acknowledge fruitful discussions with P.I. Arseyev, N.S. Maslova and V.N. Mantsevich. This work was supported by the Russian Foundation for Basic Research, Government of Krasnoyarsk Territory, Krasnoyarsk Region Science and Technology Support Fund (project nos. 16-02-00073, 17-42-240441, and 17-02-00135). The work of S.A. was supported by the Council of the President of the Russian Federation for Support of Young Scientists and Leading Scientific Schools (project no. MK-3722.2018.2). The publication was prepared by M.K. within the framework of the Academic Fund Program at the National Research University Higher School of Economy in 2017–2018 (project no. 18-05-0024) and by the Russian Academic Excellence Project "5-100."

REFERENCES

1. J. M. Elzerman, R. Hanson, J. S. Greidanus, L. H. Willems van Beveren, S. de Franceschi, L. M. K. Vandersypen, S. Tarucha, and L. P. Kouwenhoven, Phys. Rev. B **67**, 161308 (2003).
2. L. Gaudreau, S. A. Studenikin, A. S. Sachrajda, P. Zawadzki, A. Kam, J. Lapointe, M. Korkusinski, and P. Hawrylak, Phys. Rev. Lett. **97**, 036807 (2006).
3. D. Loss and D. P. DiVincenzo, Phys. Rev. A **57**, 120 (1998).
4. F. H. L. Koppens, C. Buizert, K. J. Tielrooij, I. T. Vink, K. C. Nowack, T. Meunier, L. P. Kouwenhoven, and L. M. K. Vandersypen, Nature (London, U.K.) **442**, 766 (2006).
5. M. R. Delbecq, T. Nakajima, T. Otsuka, S. Amaha, J. D. Watson, M. J. Manfra, and S. Tarucha, Appl. Phys. Lett. **104**, 183111 (2014).
6. T. Ito, T. Otsuka, S. Amaha, M. R. Delbecq, T. Nakajima, J. Yoneda, K. Takeda, G. Allison, A. Noiri, K. Kawasaki, and S. Tarucha, Sci. Rep. **6**, 39113 (2016).
7. T. Byrnes, N. Y. Kim, K. Kusudo, and Y. Yamamoto, Phys. Rev. B **78**, 075320 (2008).
8. C.-Y. Hsieh, Y.-P. Shim, M. Korkusinski, and P. Hawrylak, Rep. Prog. Phys. **75**, 114501 (2012).
9. R. Thalineau, S. Hermelin, A. D. Wieck, C. Bauerle, L. Saminadayar, and T. Meunier, Appl. Phys. Lett. **101**, 103102 (2012).
10. T. A. Baart, N. Jovanovic, C. Reichl, W. Wegscheider, and L. M. K. Vandersypen, Appl. Phys. Lett. **109**, 043101 (2016).
11. A. Oguri, Y. Nisikawa, Y. Tanaka, and T. Numata, J. Magn. Magn. Mater. **310**, 1139 (2007).
12. P. Barthelemy and L. M. K. Vandersypen, Ann. Phys. **525**, 808 (2013).
13. I. Ozfidan, A. H. Trojnara, M. Korkusinski, and P. Hawrylak, Solid State Commun. **172**, 15 (2013).
14. A. C. Johnson, J. R. Petta, C. M. Marcus, M. P. Hanson, and A. C. Gossard, Phys. Rev. B **72**, 165308 (2005).
15. C.-Y. Hsieh, Y.-P. Shim, and P. Hawrylak, Phys. Rev. B **85**, 085309 (2012).
16. D. Weinmann, W. Hausler, and B. Kramer, Phys. Rev. Lett. **74**, 984 (1995).
17. D. Urban and J. Konig, Phys. Rev. B **79**, 165319 (2009).
18. B. Michaelis, C. Emary, and C. W. J. Beenakker, Europhys. Lett. **73**, 677 (2006).
19. C. Poltl, C. Emary, and T. Brandes, Phys. Rev. B **80**, 115313 (2009).
20. N. S. Maslova, V. N. Mantsevich, and P. I. Arseev, J. Exp. Theor. Phys. **122**, 1084 (2016).

21. D. Jacob, B. Wunsch, and D. Pfannkuche, Phys. Rev. B **70**, 081314(R) (2004).
22. D. Rogovin and D. J. Scalapino, Ann. Phys. (N.Y.) **86**, 1 (1974).
23. L. V. Keldysh, Sov. Phys. JETP **20**, 1018 (1965).
24. J. Q. You and H.-Z. Zheng, Phys. Rev. B **60**, 8727 (1999).
25. M. Yu. Kagan, V. V. Val'kov, and S. V. Aksenov, Phys. Rev. B **95**, 035411 (2017).
26. M. Yu. Kagan, V. V. Val'kov, and S. V. Aksenov, J. Magn. Magn. Mater. **440**, 15 (2017).
27. C. Lacroix, J. Phys. F: Met. Phys. **11**, 2389 (1981).
28. A. Volya and V. Zelevinsky, Phys. Rev. C **67**, 054322 (2003).
29. A. F. Sadreev, E. N. Bulgakov, and I. Rotter, Phys. Rev. B **73**, 235342 (2006).
30. A. F. Sadreev and T. V. Babushkina, JETP Lett. **88**, 360 (2008).
31. P. I. Arseev, N. S. Maslova, and V. N. Mantsevich, J. Exp. Theor. Phys. **142**, 156 (2012).
32. J. Hubbard, Proc. R. Soc. London, Ser. A **281**, 401 (1964).